Multipole and plane wave expansions of diverging and converging fields

Thanh Xuan Hoang,[1,3,*] **Xudong Chen,**[1] **and Colin J. R. Sheppard**[2]

[1]*Department of Electrical and Computer Engineering, National University of Singapore, Singapore 117576, Singapore*
[2]*Istituto Italiano di Tecnologia, via Morego 30, Genova 16163, Italy*
[3]*Currently with Singapore-MIT Alliance for Research and Technology (SMART) Centre, 1 Create Way, Singapore 138602, Singapore*

[*]*hoangxuan11@gmail.com*

Abstract: This paper presents and compares two basis systems, spherical harmonics and plane waves, for studying diverging and converging beams in an optical system. We show a similarity between a converging field and the time reversed field of a radiation field. We present and analyze the differences between the Debye-Wolf diffraction integral and the multipole theory for focusing of polarized light. The Debye-Wolf diffraction integral gives a well-known anomalous behavior on the optical axis and at the edge of the focused beam that can be avoided by using the multipole theory.

OCIS codes: (110.0110) Imaging systems; (180.0180) Microscopy; (260.0260) Physical optics.

References and links

1. M. Born and W. Wolf, *Principles of Optics*, 7th ed. (Cambridge University, 2005).
2. N. I. Zheludev, "What diffraction limit?," Nat. Mater. **7**, 420–422 (2008).
3. R. P. Feynman, R. P. Leighton, and M. Sands, *The Feynman Lectures on Physics* (Addison-Wesley, 2006), Vol. II.
4. C. J. R. Sheppard, "High-aperture beams," J. Opt. Soc. Am. A **18**, 1579–1587 (2001).
5. H. Noh, S. M. Popoff, and H. Cao, "Broadband subwavelength focusing of light using a passive sink," Opt. Express **21**, 17435–17446 (2013).
6. S. Heugel, A. S. Villar, M. Sondermann, U. Peschel, and G. Leuchs, "On the analogy between a single atom and an optical resonator," Laser Phys. **20**, 100–106 (2010).
7. A. Sentenac, P. C. Chaumet, and G. Leuchs, "Total absorption of light by a nanoparticle: an electromagnetic sink in the optical regime," Opt. Lett. **38**, 818–820 (2013).
8. J. de Rosny and M. Fink, "Overcoming the diffraction limit in wave physics using a time-reversal mirror and a novel acoustic sink," Phys. Rev. Lett. **89**, 124301 (2002).
9. P. Lueg, "Process of silencing sound oscillations," US Patent No.2043416 (1936).
10. R. W. Hellwarth, "Generation of time-reversed wave fronts by nonlinear refraction," J. Opt. Soc. Am. **67**, 1–3 (1977).
11. Y. Urzhumov, C. Ciracì, and D. R. Smith, "Optical time reversal with graphene," Nat. Phys. **9**, 393–394 (2013).
12. G. Lerosey, J. de Rosny, A. Tourin, and M. Fink, "Focusing beyond the diffraction limit with far-field time reversal," Science **315**, 1120–1122 (2007).
13. J. D. Lawson, "Some attributes of real and virtual photons," Contemp. Phys. **11**, 575–580 (1970).
14. O. Keller, *Quantum Theory of Near-Field Electrodynamics* (Springer, 2011).
15. G. Leuchs and M. Sondermann, "Time reversal symmetry in optics," Phys. Scr. **85**, 058101 (2012).
16. S. Quabis, R. Dorn, M. Eberler, and G. Leuchs, "Focusing light to a tighter spot," Opt. Commun. **179**, 1–7 (2000).
17. R. Dorn, S. Quabis, and G. Leuchs, "Sharper focus for a radially polarized light beam," Phys. Rev. Lett. **91**, 233901 (2003).
18. E. Mudry, E. Le Moal, P. Ferrand, P. C. Chaumet, and A. Sentenac, "Isotropic diffraction-limited focusing using a single objective lens," Phys. Rev. Lett. **105**, 203903 (2010).

#205111 - $15.00 USD Received 20 Jan 2014; revised 12 Mar 2014; accepted 13 Mar 2014; published 7 Apr 2014

19. G. Leuchs and M. Sondermann, "Light-matter interaction in free space," J. Mod. Opt. **60**, 36-42 (2013).
20. M. Sondermann, R. Maiwald, H. Konermann, N. Lindlein, U. Peschel, and G. Leuchs, "Design of a mode converter for efficient light-atom coupling in free space," Appl. Phys. B **89**, 489–492 (2007).
21. A. Erdélyi, "Zur theorie der kugelwellen von Artur Erdélyi," Physica **IV**, 107–120 (1937).
22. A. J. Devaney and E. Wolf, "Multipole expansions and plane wave representations of the electromagnetic field," J. Math. Phys. **15**, 234–244 (1974).
23. T. X. Hoang, X. Chen, and C. J. R. Sheppard, "Multipole theory for tight focusing of polarized light, including radially polarized and other special cases," J. Opt. Soc. Am. A **29**, 32–43 (2012).
24. C. Brosseau, *Fundamentals of Polarized Light: A Statistical Optics Approach* (John Wiley, 1998).
25. Y. D. Chong, L. Ge, H. Cao, and A. D. Stone, "Coherent perfect absorbers: Time-reversed lasers," Phys. Rev. Lett. **105**, 053901 (2010).
26. W. Wan, Y. Chong, L. Ge, H. Noh, A. D. Stone, and H. Cao, "Time-reversed lasing and interferometric control of absorption," Science **331**, 889–892 (2011).
27. M. Nieto-Vesperinas, *Scattering and Diffraction in Physical Optics*, 2nd ed. (World Scientific, 2006).
28. E. Wolf, "Electromagnetic diffraction in optical systems I. An integral representation of the image field," Proc. R. Soc. London Ser. A **253**, 349–357 (1959).
29. B. Richards, "Diffraction in systems of high relative aperture," in *Astronomical Optics and Related Subjects*, Z. Kopal, ed. (North Holland, 1955).
30. B. Richards and E. Wolf, "Electromagnetic diffraction in optical systems II. Structure of the image field in an aplanatic system," Proc. R. Soc. London Ser. A **253**, 358–379 (1959).
31. T. X. Hoang, X. Chen, and C. J. R. Sheppard, "Rigorous analytical modeling of high-aperture focusing through a spherical interface," J. Opt. Soc. Am. A **30**, 1426–1440 (2013).
32. T. X. Hoang, X. Chen, and C. J. R. Sheppard, "Interpretation of the scattering mechanism for particles in a focused beam," Phys. Rev. A **86**, 033817 (2012).
33. J. A. Kong, *Electromagnetic Wave Theory* (EMW Publishing, 2008).
34. C. J. R. Sheppard, "Intermediate field behind a nanostructure," Phys. Rev. A **88**, 033839 (2013).
35. U. Leonhardt, "Perfect imaging without negative refraction," New J. Phys. **11**, 093040 (2009).
36. U. Leonhardt and T. G. Philbin, "Perfect imaging with positive refraction in three dimensions," Phys. Rev. A **81**, 011804(R) (2010).
37. R. J. Blaikie, "Comment on 'Perfect imaging without negative refraction'," New J. Phys. **12**, 058001 (2010).
38. R. Merlin, "Comment on "Perfect imaging with positive refraction in three dimensions"," Phys. Rev. A **82**, 057801 (2010).
39. U. Leonhardt, "Reply to "Comment on 'Perfect imaging with positive refraction in three dimensions' "," Phys. Rev. A **82**, 057802 (2010).
40. Y. G. Ma, S. Sahebdivan, C. K. Ong, T. Tyc, and U. Leonhardt, "Evidence for subwavelength imaging with positive refraction," New J. Phys. **13**, 033016 (2011).
41. R. Merlin, "Maxwell's fish-eye lens and the mirage of perfect imaging," J. Opt. **13**, 024017 (2011).
42. X. Zhang, "Perfect lenses in focus: No drain, no gain," Nature **480**, 42–43 (2011).
43. S. K. Rhodes, K. A. Nugent, and A. Roberts, "Precision measurement of the electromagnetic fields in the focal region of a high-numerical-aperture lens using a tapered fiber probe," J. Opt. Soc. Am. A **19**, 1689–1693 (2002).
44. J. C. Maxwell, "On the general laws of optical instruments," Q. J. Pure Appl. Math. **2**, 271 (1858).
45. J. B. Pendry, "Negative refraction makes perfect lens," Phys. Rev. Lett. **85**, 3966 (2000).
46. C. J. R. Sheppard and C. J. Cogswell, "Reflection and transmission confocal microscopy," presented at the Optics in Medicine, Biology and Environmental Research: Proceedings of the International Conference on Optics Within Life Sciences, Garmisch-Partenkirchen, Germany, 1993, 1990.
47. S. W. Hell and E. H. K. Stelzer, "Properties of a 4Pi confocal flourescence microscope," J. Opt. Soc. Am. A **9**, 2159–2166 (1992).
48. M. G. L. Gustafsson, D. A. Agard, and J. W. Sedat, "I5M: 3D widefield light microscopy with better than 100nm axial resolution," J. Microsc. **195,** 10–16 (1999).
49. A. G. Curto, T. H. Taminiau, G. Volpe, M. P. Kreuzer, R. Quidant, and N. F. van Hulst, "Multipolar radiation of quantum emitters with nanowire optical antennas," Nat. Commun. **4**, 1750 (2013).
50. G. C. Sherman and W. C. Chew, "Aperture and far-field distributions expressed by the Debye integral representation of focused fields," J. Opt. Soc. Am. **72**, 1076–1083 (1981).
51. N. G. Van Kampen, "An asymptotic treatment of diffraction problems," Physica **XIV**, 575–589 (1949).
52. M. R. Foreman, S. S. Sherif, P. R. T. Munro, and P. Török, "Inversion of the Debye-Wolf diffraction integral using an eigenfunction representation of the electric fields in the focal region," Opt. Express **16**, 4901–4917 (2008).
53. W. H. Carter, "Bandlimited angular spectrum approximation to a scalar dipole field," Opt. Commun. **2**, 142–148 (1970).
54. W. H. Carter, "Bandlimited angular spectrum approximation to a spherical scalar wave field," J. Opt. Soc. Am. **65**, 1054–1058 (1975).

#205111 - $15.00 USD Received 20 Jan 2014; revised 12 Mar 2014; accepted 13 Mar 2014; published 7 Apr 2014

1. Introduction

Diffraction phenomena have been known since the time of Leonardo da Vinci [1]. And since the time of Abbe, diffraction has been believed to be the fundamental physical phenomenon which limits the resolution of a conventional microscope [1]. However, in the last several decades we have witnessed the invention of some methods to push the capacity of imaging of a microscope beyond the diffraction limit [2]. In this paper, we decompose a diffraction field into a converging field and a diverging field, and discuss the implications of each for sub-wavelength focusing and imaging.

Feynman pointed out that both inward and outward spherical waves traveling to and from the origin are solutions of Maxwell's equations in free space [3]. In his lectures, he also briefly mentioned that only the outgoing (diverging) wave solution makes "physical sense" when describing the electromagnetic field radiated by a source. After the invention of laser, the concept of a converging wave has been mentioned more frequently, especially in light focusing systems. Many lasers produce Gaussian beams that exhibit a Gaussian variation in the waist [4]. To describe the propagation of the Gaussian beam in free space, the complex-source-point theory has been developed. The central idea of this theory is to move the source an imaginary distance z_0 from the origin so that there is no source in real space and the propagation of the beam still satisfies the Maxwell's equations. However, this complex-source-point theory results in a singularity in free space. Due to this singularity, a theory based on a source-sink pair has been proposed to avoid it ([4], and references therein). In the context of describing the propagation of the Gaussian beam, the source and the sink are purely-mathematical concepts. But the source and the sink in the context of time reversal symmetry have represented an active research topic for the last two decades and have been accepted widely as physical concepts. The sinks can be categorized into two types, i.e., passive sinks and active sinks, respectively. A passive sink absorbs energy and its physical mechanism has been explained in different contexts [5–7]. The physical mechanism of an active sink is to radiate a wave that destructively interferes completely with the resultant diverging wave of the converging wave. The active sink has been demonstrated in acoustic wave experiments, and has been exploited commercially in noise cancellation [8, 9].

The source shown in Fig. 1 radiates a wave propagating towards infinity. If the propagation direction of the radiated wave is reversed in all degrees of freedom - for example, by a process of phase conjugating the radiated field using a nonlinear material [10], metamaterial, or graphene [11]- we will have a converging wave approaching back to the position of the source. Now, we

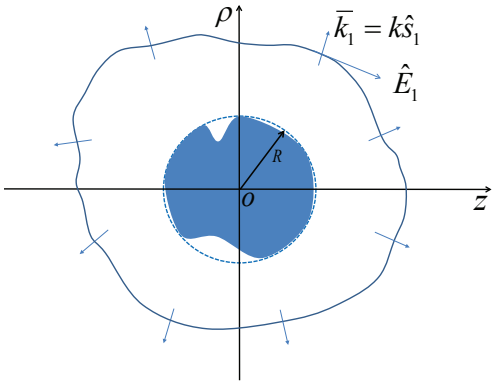

Fig. 1. Source radiates a wave propagating towards infinity.

#205111 - $15.00 USD Received 20 Jan 2014; revised 12 Mar 2014; accepted 13 Mar 2014; published 7 Apr 2014

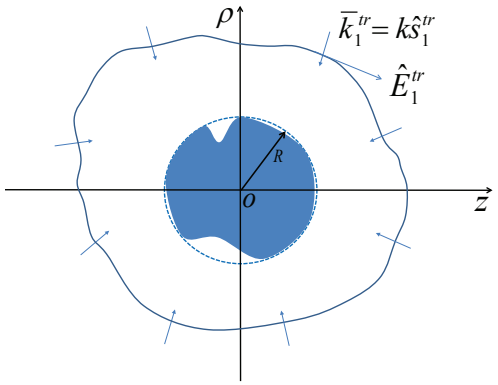

Fig. 2. A sink absorbs a wave converging from infinity.

consider the case in which the source is removed and hence the region around the origin is a source-free region. Due to energy flux conservation, there must be a diverging wave following the converging wave. And the total field in the source-free region is due to the interference of these two beams. It has been shown that the interference results in a focal spot which is subject to the diffraction limit [5, 12]. As a quantum mechanism, the nature of photons is the reason behind the diffraction limit that can be explained in terms of the Heisenberg uncertainty principle. The principle says that the spatial confinement of a photon, i.e. the focal spot, is inversely proportional to its momentum spread [11]. However, if the source is replaced by the time reversed source as shown in Fig. 2, which, in a more general context, is a sink, the converging wave will be absorbed completely. The energy of the converging wave is converted into two parts when approaching the sink: the energy of non-propagating field and the absorbed energy. The non-propagating field, or equivalently the evanescent field, is associated with large or complex k-vectors [13], which are believed to be necessary for producing a sub-diffraction limit spot at the focus. In the particle-like manifestations of the electromagnetic field, Ole Keller developed new equations to study photon wave mechanics and used the concept of the photon embryo to describe the evanescent field [14]. This evanescent field is also referred to as a localized field.

Due to the simplicity in explaining various phenomena relating to the light focusing, the time reversal symmetry has gained much attention from many researchers in recent years [15]. Under the guidance of time reversal symmetry, Quabis and colleagues predicted that using a radially polarized beam produces a tighter focal spot in comparison with a linearly polarized beam [16]. This prediction was later confirmed by Dorn et. al. [17]. Similarly, under this guidance, Mudry et. al. improved the performance of confocal microscopy to obtain a 4Pi microscope with a combination of a spatial light modulator, a single microscope objective, and a mirror [18]. Light-matter interaction between a focused beam and a quantum target is also usually studied and explained in the context of time reversal symmetry [19, 20].

2. Theory

In this paper, we derive fields representing a source and a sink based on plane waves and spherical harmonics. We then employ the general field expressions to discuss the two methods, the Debye-Wolf diffraction integral and multipole theory, for evaluating the focal field of an aplanatic system shown in Fig. 3.

#205111 - $15.00 USD Received 20 Jan 2014; revised 12 Mar 2014; accepted 13 Mar 2014; published 7 Apr 2014

Here, we use the definitions of the vectorial multipole fields as follows:

$$\mathbf{N}_{lm}(\bar{r}) = \nabla \times \nabla \times [\bar{r}\Lambda_{lm}(\bar{r})],$$
$$\mathbf{M}_{lm}(\bar{r}) = ik\nabla \times [\bar{r}\Lambda_{lm}(\bar{r})],$$

where the scalar multipole Debye potential Λ_{lm} represents $\bigwedge_{lm}$, $\prod_{lm}^{(1)}$, and $\prod_{lm}^{(2)}$ that are shown in Eqs. (1), (2), and (3), respectively [21]:

$$\bigwedge_{lm}(\bar{r}) = j_l(kr)Y_l^m(\theta,\phi) = C_l^m \left\{ \left[\frac{1}{ik}\left(\frac{\partial}{\partial x} + i\frac{\partial}{\partial y}\right)\right]^m P_l^{(m)}\left(\frac{1}{ik}\frac{\partial}{\partial z}\right)\right\} \frac{\sin(kr)}{kr}, \tag{1}$$

$$\prod_{lm}^{(1)}(\bar{r}) = h_l^{(1)}(kr)Y_l^m(\theta,\phi) = C_l^m \left\{ \left[\frac{1}{ik}\left(\frac{\partial}{\partial x} + i\frac{\partial}{\partial y}\right)\right]^m P_l^{(m)}\left(\frac{1}{ik}\frac{\partial}{\partial z}\right)\right\} \frac{e^{ikr}}{ikr}, \tag{2}$$

$$\prod_{lm}^{(2)}(\bar{r}) = h_l^{(2)}(kr)Y_l^m(\theta,\phi) = C_l^m \left\{ \left[\frac{1}{ik}\left(\frac{\partial}{\partial x} + i\frac{\partial}{\partial y}\right)\right]^m P_l^{(m)}\left(\frac{1}{ik}\frac{\partial}{\partial z}\right)\right\} \frac{e^{-ikr}}{-ikr}. \tag{3}$$

It is obvious that $\prod_{lm}^{(1)}(\bar{r}) + \prod_{lm}^{(2)}(\bar{r}) = 2\bigwedge_{lm}(\bar{r})$. The scalar multipole field $\bigwedge_{lm}(\bar{r})$ is appropriate for a description of a source-free monochromatic scalar wave field [22]. On the other hand, $\prod_{lm}^{(1)}(\bar{r})$ and $\prod_{lm}^{(2)}(\bar{r})$ are appropriate for descriptions of a monochromatic scalar wave field in presence of a localized source distribution or a localized sink distribution, respectively.

Now, we consider a real, monochromatic, electromagnetic field $\bar{E}_1(\bar{r},t) = Re\{\bar{E}_1(\bar{r})e^{-i\omega t}\}$ generated by a charge-current distribution as shown in Fig. 1:

$$\rho_1(\bar{r},t) = Re\{\rho_1(\bar{r})e^{-i\omega t}\}, \bar{J}_1(\bar{r},t) = Re\{\bar{J}_1(\bar{r})e^{-i\omega t}\}.$$

If the source ($\rho_1(\bar{r})$ and $\bar{J}_1(\bar{r})$) is continuous and a continuously differentiable function of position, and vanishes identically outside a sphere of radius R, we can show the radiation field due to the source to be [22]:

$$\bar{E}_1(\bar{r}) = \frac{ik_1}{2\pi}\int_0^{2\pi} d\beta_1 \int_{C^{\pm}} d\alpha_1 \sin\alpha_1 \hat{E}_1(\hat{s}_1) e^{i\bar{k}_1.\bar{r}}, \tag{4}$$

where the spectral amplitude vector $\hat{E}_1(\hat{s})$ is given by

$$\hat{E}_1(\hat{s}_1) = \int_{|\vec{r}'|\le R} \left[i\frac{k_1}{c}\bar{J}_1(\vec{r}') - \nabla\rho_1(\vec{r}')\right] e^{-i\bar{k}_1.\vec{r}'}\, d^3\vec{r}'. \tag{5}$$

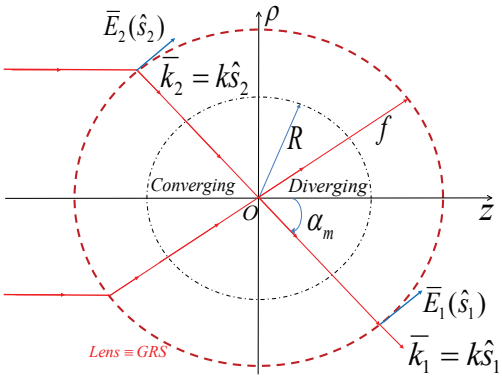

Fig. 3. Gaussian reference sphere represents an aplanatic focusing system.

#205111 - $15.00 USD Received 20 Jan 2014; revised 12 Mar 2014; accepted 13 Mar 2014; published 7 Apr 2014

Here the integral contours are shown in Fig. 4, and C^+ (D^+) and C^- (D^-) are used for the regions $z>0$ and $z<0$, respectively. Equation (4) expresses the electric field in terms of plane waves, and equivalently the electric field can be expressed in terms of vectorial multipole fields $\mathbf{N}_{lm}$ and $\mathbf{M}_{lm}$ as follows [22, 23]:

$$\bar{E}_1(\bar{r}) = \sum_{l=1}^{\infty}\sum_{m=-l}^{l}[g_{El}^m \mathbf{N}_{lm}^{(1)}(\bar{r}) + g_{Ml}^m \mathbf{M}_{lm}^{(1)}(\bar{r})], \tag{6}$$

where the strengths of the multipoles g_{El}^m and g_{Ml}^m are

$$g_{El}^m = \frac{i^{l+1}}{l(l+1)}\int_0^{2\pi}\int_0^{\pi}(\hat{E}_1(\hat{s}_1)\times\hat{s}_1)\cdot\mathbf{Y}_l^{m^*}(\alpha_1,\beta_1)\sin\alpha_1\, d\alpha_1\, d\beta_1, \tag{7}$$

$$g_{Ml}^m = \frac{i^{l+1}}{l(l+1)}\int_0^{2\pi}\int_0^{\pi}\hat{E}_1(\hat{s}_1)\cdot\mathbf{Y}_l^{m^*}(\alpha_1,\beta_1)\sin\alpha_1\, d\alpha_1\, d\beta_1. \tag{8}$$

We can obtain the time-reversed field $\bar{E}_1^{tr}(\bar{r})$ of the radiated field $\bar{E}_1(\bar{r})$ by applying the phase conjugation to the vectorial field in Eq. (6):

$$\bar{E}_1^{tr}(\bar{r}) = \sum_{l=1}^{\infty}\sum_{m=-l}^{l}[g_{El}^{m*}\mathbf{N}_{lm}^{(2)}(\bar{r}) - g_{Ml}^{m*}\mathbf{M}_{lm}^{(2)}(\bar{r})]. \tag{9}$$

For complete absorption of the time-reversed field, the sink, which is the time-reversed source, must comprise the charge-current distribution $(\rho_1(\bar{r},-t), \bar{J}_1(\bar{r},-t))$ [24]. More details on the sink can be obtained in [5, 7, 25, 26]. Now, we consider the case in which the time-reversed field approaches the focus without a sink. Due to energy flux conservation, there must be a diverging wave from the focus following the converging wave [12]. For convenience, we denote the converging wave $\bar{E}_2(\bar{r})$ and the diverging wave $\bar{E}_1(\bar{r})$ as shown in Fig. 3. For the converging wave, we can show that [27]:

$$\bar{E}_2(\bar{r}) = -\frac{ik_2}{2\pi}\int_0^{2\pi} d\beta_2 \int_{D^{\pm}} d\alpha_2 \sin\alpha_2 \hat{E}_2(\hat{s}_2) e^{i\bar{k}_2\cdot\bar{r}}. \tag{10}$$

Equivalently, we can express the fields in terms of vectorial multipole fields $\mathbf{N}_{lm}^{(2)}$ and $\mathbf{M}_{lm}^{(2)}$ as follows [22, 23]:

$$\bar{E}_2(\bar{r}) = \sum_{l=1}^{\infty}\sum_{m=-l}^{l}[q_{El}^m \mathbf{N}_{lm}^{(2)}(\bar{r}) + q_{Ml}^m \mathbf{M}_{lm}^{(2)}(\bar{r})], \tag{11}$$

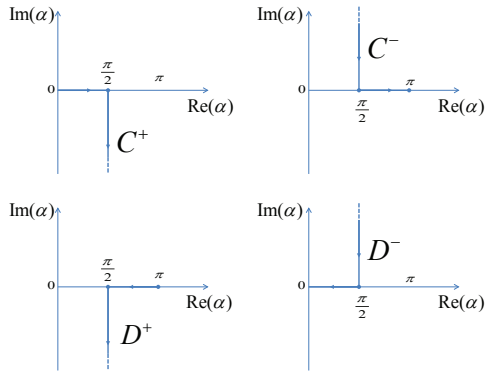

Fig. 4. Integration contours.

#205111 - $15.00 USD Received 20 Jan 2014; revised 12 Mar 2014; accepted 13 Mar 2014; published 7 Apr 2014

where the strengths of the multipoles q_{El}^m and q_{Ml}^m can be evaluated using Eq. (7) and Eq. (8), respectively, by replacing $(\hat{E}_1, \hat{s}_1, \alpha_1, \beta_1)$ with $(\hat{E}_2, \hat{s}_2, \alpha_2, \beta_2)$. As observed in Fig. 3, we have $\hat{E}_1 = \hat{E}_2 = \hat{E}$ and $k_1 = k_2 = k$. As a result, we have $q_{El}^m = g_{El}^m = p_{El}^m$ and $q_{Ml}^m = g_{Ml}^m = p_{Ml}^m$. Hence, without the sink the total field will be the interference between the converging field E_2 and the diverging field E_1:

$$\begin{aligned} \bar{E}(\bar{r}) &= \bar{E_1}(\bar{r}) + \bar{E_2}(\bar{r}) \\ &= 2\sum_{l=1}^{\infty}\sum_{m=-l}^{l}[p_{El}^m \mathbf{N}_{lm}(\bar{r}) + p_{Ml}^m \mathbf{M}_{lm}(\bar{r})]. \end{aligned} \tag{12}$$

Equation (12) expresses the focal field in terms of the vectorial multipole fields. Equivalently, we can express the focal field in terms of the plane waves by adding Eq. (4) and Eq. (10):

$$\bar{E}(\bar{r}) = \frac{ik}{2\pi}\int_0^{2\pi} d\beta \int_0^{\pi} d\alpha \sin\alpha \hat{E}(\hat{s}) e^{i\bar{k}.\bar{r}}. \tag{13}$$

Whereas the representation in Eq. (13) can be considered as Whittaker's representation for the source-free field which expands the field in terms of the plane waves traveling in all directions, the representations in Eq. (4) and Eq. (10) can be considered as Weyl's representation for diverging and converging fields, respectively [22].

3. Simulations and discussions

An aplanatic focusing system is represented by a Gaussian reference sphere (GRS) as shown in Fig. 3. To evaluate the focal field, we can use either Eq. (12) or Eq. (13). As we derive above, the two equations are equivalent and hence in no way give different results. However the above formulas are for a diverging field and a converging field over a full solid angle, but practically we more often encounter the case of a field converging and diverging from a partial solid angle. For example, we often focus light using an aplanatic system with a finite focal length f and an illumination semi-angle $\alpha_m < \frac{\pi}{2}$. For this particular case, we need to make some assumptions and some approximations before we can apply Eq. (12) and Eq. (13). This section is devoted to study the focused field of the aplanatic system.

Based on the plane wave expansions, Debye derived an elegant formula for treating the diffraction caused by a small aperture for the scalar case in 1909. In 1959, Wolf generalized the formula by including the effect of the vectorial nature of the field ([28], and references therein). Richards and Wolf used the formula for estimating the focal field of an aplanatic system [29, 30]. In this paper, we call the formula the Debye-Wolf diffraction integral (DI). As an alternative to the DI, the multipole theory based on the multipole expansions has been developed and used [23, 31, 32]. We call the formula based on the multipole theory the multipole theory method (MTM). We have showed that DI and MTM give a perfect agreement on the electric intensity around the focus in [23]. However, there are interesting differences between the two methods which are presented in this paper.

First, we consider a Hertzian electric dipole with the current dipole moment Il pointing in the $\hat{z}$ direction and located at the origin. We can show that the spectral amplitude vector of the radiation field of the dipole is [33]:

$$\hat{E}_1(\hat{s}_1) = -\frac{i\omega\mu Il}{4\pi}\sin(\alpha_1)\hat{\alpha}_1, \tag{14}$$

where ω is the angular frequency of the oscillation of the dipole. Substituting Eq. (14) into Eq. (7) and Eq. (8), we can show that only $g_{E1}^0 \neq 0$ and that $g_{E1}^0 = \frac{\omega\mu Il}{2\sqrt{3\pi}}$. Hence, the radiation field

#205111 - $15.00 USD Received 20 Jan 2014; revised 12 Mar 2014; accepted 13 Mar 2014; published 7 Apr 2014

$\bar{E}_1$ and its time reversed field $\bar{E}_1^{tr}$ are as follows:

$$\bar{E}_1(\bar{r}) = g_{E1}^0 \mathbf{N}_{10}^{(1)}, \tag{15}$$

$$\bar{E}_1^{tr}(\bar{r}) = g_{E1}^0 \mathbf{N}_{10}^{(2)}. \tag{16}$$

There are different approaches for producing the time reversed field, for example, using a massive array of sensors [12], a mode converter [20], or a combination of an objective lens, spatial light modulator, and a mirror [18]. For convenience, we denote the time reversed field $\bar{E}_1^{tr}$ as a converging field $\bar{E}_2$. Now, we consider the case of absence of the sink at the origin. The converging field from the full solid angle is equivalent to converging from the whole GRS $\alpha_m = \pi$ as shown in Fig. 3. As explained in the previous sections, the focal field is evaluated using Eq. (12):

$$\bar{E}(\bar{r}) = 2g_{E1}^0 \mathbf{N}_{10}. \tag{17}$$

Figure 5 shows a contour plot of electric energy density using Eq. (17). In this full solid angle of convergence, the full widths at half maximum (FWHM) in the transversal direction and the longitudinal direction are $\frac{\lambda}{2.48}$ and $\frac{\lambda}{1.73}$, respectively. These values of FWHM are very close to the usually assumed classical resolution limit of $\frac{\lambda}{2}$ [34]. In fact, the convergence from a full solid angle has been known and investigated as a special ability of a fish eye lens since the time of Maxwell [1]. Maxwell is attributed to be the first one to investigate the fish eye lens, and hence the name of Maxwell's fish eye lens is usually used. Leonhardt recently proposed that Maxwell's fish eye lens can be used as a perfect lens [35, 36]. It is interesting to note that in his first papers he did not mention the necessity for a drain, or sink. After two critical comments on two different papers [37, 38], he took the necessity for a drain on board [39], and even experimentally demonstrated his approach using a drain for microwaves in a two-dimensional setup [40]. However, extension to three dimensions might prove difficult due to accessibility issues. Merlin [41] and Zhang [42] both consider this method to be really just an example of time-reversal. Alternatively, we can think of it as being an example of near-field microscopy, where in this case 'near-field' refers to image space, rather than the usual object space. In fact near-field probes have already been used to investigate focused fields [43]. Near-field imaging brings several drawbacks, however, that are also important for the current case, especially the interaction of the probe with the focused field, i.e. the probe disturbing the field that is being measured, which is exactly what Leonhardt's approach requires. Maxwell's fish

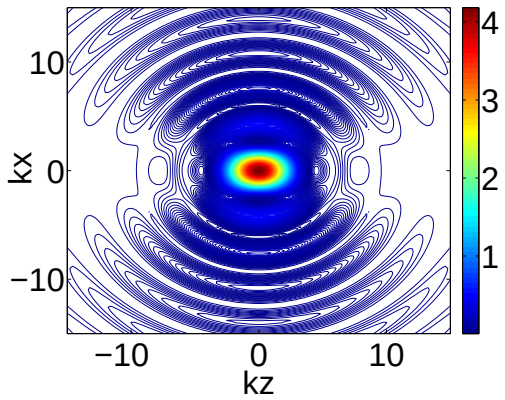

Fig. 5. Contour plot of electric energy density due to the time reversed field in absence of the sink.

#205111 - $15.00 USD Received 20 Jan 2014; revised 12 Mar 2014; accepted 13 Mar 2014; published 7 Apr 2014

eye has a magnification of unity. In fact Maxwell proved that in order to image a 3D region perfectly the magnification must be unity [44]. This may be a big disadvantage (which is also shared by Pendry's super-lens [45]), as if the image is only as large as the object, why bother with the image? There may be also other ways of achieving the aberration-free focusing part of Leonhardt's scheme, other than using a Maxwell fish eye. Surprisingly, no one seems to have mentioned the similarity with 4Pi microscopy, which uses two opposed high numerical aperture microscope objectives [46, 47]. 4Pi microscopy is performed as a scanning technique, but the corresponding non-scanning technique has also been demonstrated [48]. 4Pi focusing would seem a viable alternative to the Maxwell's fish eye, with some practical advantages such as ease of setting up, magnification greater than unity, and the ability to access the image space. In absence of the drain at the focus, Fig. 5 represents the focal electric field intensity of 4Pi microscopy due to focusing the electric dipole field. Use of a single atom as the drain in 4π-illumination has been proposed and studied extensively by Leuchs and colleagues [15, 16, 19, 20]. It is worth noting that convergence from a full solid angle is necessary for the atom to act as a perfect absorber. For convergence from a partial solid angle, an integration between the atom and an optical antenna [49] may be needed to absorb the converging field perfectly due to the existence of higher multipole terms like quadrupole, octupole, etc. [23]. In the presence of the drain at the focus, the focal field is now represented by Eq. (16) which contains both propagating and evanescent fields. One will observe that the amplitude of the focal field keeps increasing when approaching the focus and stops only when finally reaching atomic dimension [16]. Labeling a specimen with particles that act as drains, and observing them in a 4π setup would then give perfect imaging. However, we would like to emphasize again that the focal field in this scenario represents the interaction between the probe and the focused beam, which is well understood in near-field microscopy. Leonhardt proposed a similar idea, that the drain (outlet or sink) could be 'part of a CCD array used to detect the field or a photosensitive molecule' [39]. In summary, we may identify that the drain is the key element of Leonhardt's super-resolving system, not the Maxwell's fish eye.

Now, we consider the beam converging from a partial solid angle, which we call an axial dipole wave (ADW) [23]. Ignoring the constant term $-\frac{i\omega\mu Il}{4\pi f e^{ikf}}$, the electric field on the GRS is:

$$\bar{E}_2^f = a(\alpha)\hat{\alpha}, \tag{18}$$

where

$$a(\alpha) = \sin\alpha \text{ for } \alpha \leq \alpha_m; \text{ and } a(\alpha) = 0 \text{ for } \alpha > \alpha_m.$$

For a lens with a large focal length f, we have the relation between the electric field $\bar{E}_2^f$ and the spectral amplitude vector $\hat{E}_2$ as follows [28, 31]:

$$\hat{E}_2 = f e^{ikf} \bar{E}_2^f. \tag{19}$$

In terms of ray optics, the spectral amplitude vector is usually referred to as the strength factor of the associated ray [28]. The strength factor does not change along the ray. Although it is well-known that ray optics, and consequently the concept of the strength factor, is not valid around the focus of the focusing system, it is a valid and convenient concept in the region far away from the focus. For example, on a sphere with radius $R \gg \lambda$, the concept of the strength factor can be used. And hence applying Eq. (19), we can derive the electric field on the sphere with radius R in the context of ray optics as follows:

$$\bar{E}_2^R = e^{ik(f-R)} \frac{f}{R} \bar{E}_2^f = e^{ik(f-R)} \frac{f}{R} a(\alpha)\hat{\alpha}. \tag{20}$$

In this paper, we refer to the method using Eq. (20) for evaluating the electric field as the geometrical optics method (GOM).

#205111 - $15.00 USD Received 20 Jan 2014; revised 12 Mar 2014; accepted 13 Mar 2014; published 7 Apr 2014

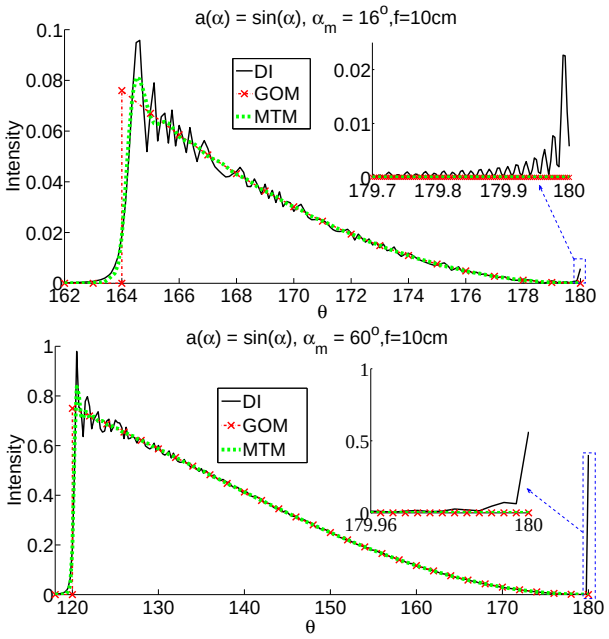

Fig. 6. Electric intensity distributions on the GRS with a low numerical aperture beam (upper) and a high numerical aperture beam (lower) with $L = 400$.

Before we analyze simulation results of the focused field using the DI, MTM, and GOM, it is worth reviewing and highlighting the differences among the three methods. All three methods assume that the field incident on the GRS is perfectly tangent to the GRS. This assumption introduces an error of the order $(kf)^{-2}$ to the assumed field in Eq. (18). For the DI, Debye showed that a peculiar behavior of the integrals exists on the optical axis in the far-region, without giving an explanation [50]. Later, in his lecture, Sommerfeld argued that the behavior was similar to the Poisson spot occurring in the diffraction pattern of a circular disk [50]. In an asymptotic treatment of the diffraction problem, Van Kampen showed that there were three kinds of the critical points [51], which contributed to the diffraction field. The first kind consists of all critical points in the diffraction aperture but not at the periphery of the aperture. The second kind consists of all the points on the periphery but not at a corner, and the third kind consists of all the corners of the aperture. For a circular aperture, there are only the first kind and second kind of the critical points. In the derivation of DI, the authors used the principle of stationary phase, i.e. they take into account only the first kind of critical points. However, the second kind of critical point is known to contribute significantly to the diffraction field around the optical axis and the shadow boundary behind the aperture [50]. In contrast to the DI, the MTM does not use the principle of stationary phase, but an error comes from truncating the double infinite summations in Eq. (11) and Eq. (12). The truncation error in MTM is similar to the error in modeling a sharp step using a finite number of Fourier terms. The error in GOM is from using ray optics to describe the propagation of the wave.

The electric intensity distributions on the GRS for a low-aperture beam $\alpha_m = 16^o$ and a high-aperture beam $\alpha_m = 60^o$ are shown in Fig. 6, in which $\theta = 180^o - \alpha$. All simulation results in this paper were obtained assuming the wavelength of the focused beam $\lambda = 1.34\mu m$. We assume the starting field on the GRS as the far field and hence the GOM is expected to describe an ideal distribution on the GRS. For the plot using DI, we observe the peculiar behavior on the

#205111 - $15.00 USD Received 20 Jan 2014; revised 12 Mar 2014; accepted 13 Mar 2014; published 7 Apr 2014

optical axis as mentioned by Debye [50]. The oscillation in the DI plot is due to excluding the contribution of the periphery of the aperture which hence causes the strong oscillation around the hard edge. There is no peculiar behavior for the plot using the MTM and there is a smaller oscillation at the hard edge compared with the DI plot. The oscillation in the MTM plot is due to the truncation of the infinite summation. The difference may be important in the inverse problem of diffraction, in which given a focal field one must design the incident field on the GRS [52]. Figure 7 shows the electric intensity distributions on spheres of different radius. We can observe that when the beam approaches the focus, the distributions using DI and MTM converge and give a perfect agreement on the sphere with $R = 0.1cm$. This is due to the fact that the contribution of the critical points of the second kind is ignorable and a smaller number of multipole terms are needed for accurately describing the focused beam. We also observe a significant deviation of the distributions using DI and MTM from the distribution using the GOM on the sphere $R = 0.2cm$. This deviation is due to the assumption of GOM that the rays travel without interference.

To compare the three methods in absence of the contribution of the periphery of the aperture, we change the apodization of the incident beam in Eq. (18) to $a(\alpha) = \sin(3\alpha)$ and take the maximum illumination angle as $\alpha_m = 60^o$. Hence, we have $a(\alpha_m) = 0$, which means there is no contribution of the critical points of the second kind to the focused field [50]. Figure 8 shows the perfect agreement of the three methods on the electric intensity distributions on the GRS. There is no oscillation caused by the truncation in the MTM because only a finite number multipole terms $L = 100$ is needed for modeling the soft edge, just like modeling a soft step using a finite number of Fourier terms. We observe an important difference between the DI plot and the MTM plot, that the DI represents the interference between the converging and diverging beams but the MTM represents only the converging beam. The DI plot for $0^o < \theta < 60^o$ represents the diverging beam. This difference is important in explaining the scattering

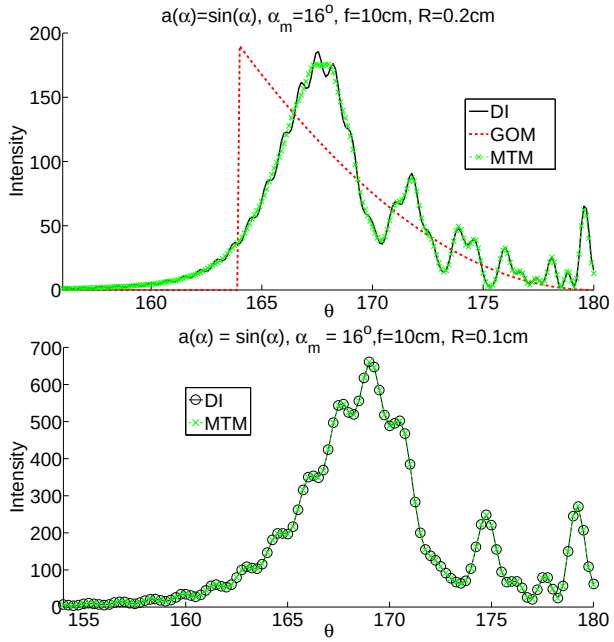

Fig. 7. Electric intensity distributions on spheres of different radius $R = 0.2cm$ (top) and $R = 0.1cm$ (bottom) with $L = 400$.

#205111 - $15.00 USD Received 20 Jan 2014; revised 12 Mar 2014; accepted 13 Mar 2014; published 7 Apr 2014

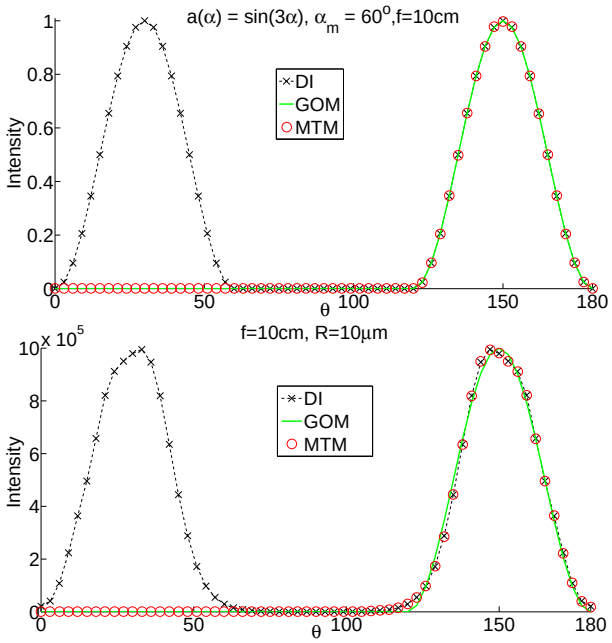

Fig. 8. Electric intensity distributions on the GRS (top) with $L = 100$ and on a sphere (bottom) $R = 10\mu m$ with L=50.

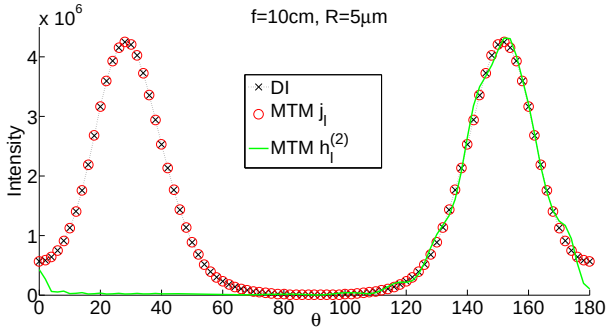

Fig. 9. Electric intensity distribution on a sphere $R = 5\mu m$ with L=30.

mechanism by spherical particles in a focused beam [32]. For this special case, geometrical optics can approximate the field on the sphere $R = 10\mu m$, giving results very close to those from DI and MTM. Figure 9 plots the electric intensity distribution on the sphere $R = 5\mu m$ in which the red circle plot is obtained by using Eq. (12) and the green plot is obtained by using Eq. (11). The red circle plot represents the interference between the converging beam and the diverging beam and hence agrees with the DI over the whole range of θ. The green plot represents the converging beam only and hence leads to a small deviation from the other two plots around the focus. This deviation represents the contribution of the inhomogeneous part of the converging beam and has been discussed in [53, 54].

#205111 - $15.00 USD Received 20 Jan 2014; revised 12 Mar 2014; accepted 13 Mar 2014; published 7 Apr 2014

4. Conclusion

In conclusion, we have derived and studied the multipole expansions and the plane wave expansions of a diverging field, a time-reversed field, and a converging field. We show the similarity between the converging field and the time reversed field of the radiated field. We have also made a comparison between the Debye-Wolf diffraction integral and the multipole theory in evaluating the focal field. The Debye-Wolf diffraction integral describes the interference between a converging beam and its associated diverging beam and ignores the contribution of the critical points of the second kind. The multipole theory decomposes the focused beam into a converging beam and a diverging beam, and introduces an error in evaluating the far field due to the truncation of the infinite summations. Our theory may find applications in the time reversal analysis and the light-matter interaction.

Acknowledgments

This research is supported by the National Research Foundation, Prime Ministers Office, Singapore under its Competitive Research Programme (CRP Award No. NRF2012NRF-CRP001-040).

#205111 - $15.00 USD Received 20 Jan 2014; revised 12 Mar 2014; accepted 13 Mar 2014; published 7 Apr 2014